Chapter 4
Numerical Study of a High Order 3D FEM-Level Set Approach for Immiscible Flow Simulation

Stefan Turek, Otto Mierka, Shuren Hysing, and Dmitri Kuzmin

Abstract Numerical simulation of incompressible multiphase flows with immiscible fluids is still a challenging field, particularly for 3D configurations undergoing complex topological changes. In this paper, we discuss a 3D FEM approach with high-order Stokes elements (Q_2/P_1) for velocity and pressure on general hexahedral meshes. A discontinuous Galerkin approach with piecewise linear polynomials (dG(1)) is used to treat the Level Set function. The developed methodology allows the application of special redistancing algorithms which do not change the position of the interface. We explain the corresponding FEM techniques for treating the advection steps and surface tension effects, and validate the corresponding 3D code with respect to both numerical test cases and experimental data. The corresponding applications describe the classical rising bubble problem for various parameters and the generation of droplets from a viscous liquid jet in a coflowing surrounding fluid. Both of these applications can be used for rigorous benchmarking of 3D multiphase flow simulations.

Keywords Multiphase flow · Finite elements · Discontinuous Galerkin · Numerical simulation

S. Turek (✉) · O. Mierka
Institut für Angewandte Mathematik, TU Dortmund, Vogelpothsweg 87, 44227 Dortmund, Germany
e-mail: ture@featflow.de

O. Mierka
e-mail: omierka@math.uni-dormtund.de

S. Hysing
Department of Mathematics, Shanghai Jiaotong University, Shanghai, China
e-mail: shuren.hysing@sjtu.edu.cn

D. Kuzmin
Lehrstuhl für Angewandte Mathematik III, Universität Erlangen-Nürnberg, Cauerstraße 11, 91058 Erlangen, Germany
e-mail: kuzmin@am.uni-erlangen.de

S. Repin et al. (eds.), *Numerical Methods for Differential Equations, Optimization, and Technological Problems*, Computational Methods in Applied Sciences 27,
DOI 10.1007/978-94-007-5288-7_4, © Springer Science+Business Media Dordrecht 2013

4.1 Introduction

Multiphase flow problems are very important in many applications, and performing accurate, robust and efficient numerical simulations of them has been the object of numerous research and simulation projects for several years. One of the main challenges for the underlying numerical methods is that the position of the moving interface between two fluids is unknown and must be determined as a part of the boundary value problem which should be solved. If we assume a domain Ω with two immiscible fluids, then the time-dependent subdomains $\Omega_1(t)$ and $\Omega_2(t)$ are bounded by an external boundary Σ and a dynamic interior boundary or interface $\Gamma(t)$ which might consist of several components (see Fig. 4.1).

Then, the usual model for laminar (multiphase) flow is described by the incompressible Navier-Stokes equations

$$\rho(\mathbf{x})\left[\frac{\partial \mathbf{u}}{\partial t}+\mathbf{u}\cdot\nabla\mathbf{u}\right]-\nabla\cdot\left(\mu(\mathbf{x})\left[\nabla\mathbf{u}+(\nabla\mathbf{u})^T\right]\right)+\nabla p=\rho(\mathbf{x})\mathbf{g}+\mathbf{f}_\Gamma(\sigma), \quad (4.1)$$

$$\nabla\cdot\mathbf{u}=0 \quad \text{in } \Omega=\Omega_1\cup\Gamma\cup\Omega_2, \quad (4.2)$$

which contain an additional force term $\mathbf{f}_\Gamma(\sigma)$ due to the surface tension σ at the free interface Γ. Here, the density ρ as well as the viscosity μ are variable and discontinuous, that is

$$\rho(\mathbf{x},t)=\begin{cases}\rho_1, & \forall\mathbf{x}\in\Omega_1(t),\\ \rho_2, & \forall\mathbf{x}\in\Omega_2(t),\end{cases}\qquad \mu(\mathbf{x},t)=\begin{cases}\mu_1, & \forall\mathbf{x}\in\Omega_1(t),\\ \mu_2, & \forall\mathbf{x}\in\Omega_2(t),\end{cases} \quad (4.3)$$

which significantly influences the velocity $\mathbf{u}$ as well as the pressure p.

This contribution describes the numerical analysis and application of a new Level Set approach in the framework of the Finite Element Method (FEM) for such multiphase flow problems. For this reason the open-source CFD package FEATFLOW (www.featflow.de) was utilized and extended with the corresponding newly created Level Set module so that the existing methodology of the FEATFLOW approach, namely flexible, high order FEM discretization schemes in space and time with flux correction [34] and edge-oriented stabilization techniques [62], unstructured meshes with adaptive grid deformation, efficient Newton-Multigrid solvers, and parallelization based on domain decomposition could be directly exploited.

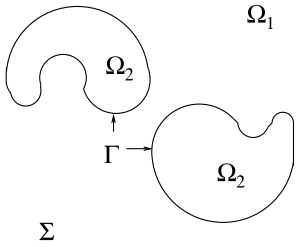

Fig. 4.1 A sketch of the complete domain $\Omega=\Omega_1\cup\Gamma\cup\Omega_2$

The outline of the paper is as follows: after a short description in Sect. 4.2 of the state-of-the-art regarding interface tracking and capturing methods, particularly for Level Set approaches, we describe in Sect. 4.3 the chosen solution technique which is based on a discrete projection method [60, 61] for the Navier–Stokes equations, the Level Set advection equation, and the corresponding reinitialization procedure. Moreover, the discretization aspects regarding the incompressible Navier–Stokes equations using the Crank–Nicolson method and the Q_2/P_1 element pair are discussed in Sect. 4.3, too, whereas the details of the employed Discontinuous Galerkin FEM approach with P_1 elements for the Level Set equation can be found in Sect. 4.4. Section 4.5 presents several numerical results which first of all evaluate the grid-independent behaviour of the developed CFD solver.

Furthermore, based on experimental and computational studies, we propose and discuss new benchmark configurations for prototypical 3D multiphase flows which can be used for 'simple' validation and evaluation of multiphase flow CFD codes without the necessity of complex postprocessing operations. Finally, the results are summarized in Sect. 4.6 where an outlook is provided for more complex 3D multiphase flow problems.

4.2 Mathematical Model

The free interface Γ is constantly being deformed and moved so that its position has to be treated as unknown and determined in every time step. Depending on the technique for the representation of the interface, one can distinguish between *front tracking* and *front capturing* approaches which can be realized on fixed as well as dynamic moving meshes. For an overview of existing numerical approaches and their classification, we recommend [52, 56]. The "natural" front tracking approach [21, 41, 55, 65] is based on an explicit tracing of the dynamic interface between the two phases. Here, in the case of Lagrangian finite element methods [25], the underlying mesh has to be constantly adapted to the free interface so that the grid points move with the interface. More flexibility is promised by the *Arbitrary Lagrangian Eulerian* (ALE) formulation [1, 2, 7, 17, 19, 51] which is based on local grid adaptation and which provides excellent results in the case of moderate deformations (for instance for small waves at the free surface). Moreover, there are many more techniques of fictitious domain and Chimera type which allow the highly accurate tracking of the dynamic interfaces via overlapping surface meshes [26]. However, such front tracking methods do not allow large deformations of the free interfaces or even topological changes such as drop formation and bubble breakup or coalescence, which typically lead to highly distorted meshes. Moreover, the computational costs regarding the implementation and also CPU timings are often very large for complex 3D simulations.

In contrast to such Lagrangian methods, Eulerian front capturing methods are much more robust and flexible. They are applicable even to free interface problems with significant topology changes (breakup of bubbles, fragmentation, coalescence,

etc.). Based on the early Marker-and-Cell method of Harlow and Welch [67], the implicit reconstruction of the interface is based on an indicator function $\phi(\mathbf{x}, t)$ which contains the information about the corresponding subdomain for the point $\mathbf{x}$ at time t. The distribution in the complete domain Ω can then be calculated via the scalar transport equation

$$\frac{\partial \phi}{\partial t} + \mathbf{u} \cdot \nabla \phi = 0 \tag{4.4}$$

so that the exact position of the free interface $\Gamma(\phi)$ at any time can be reconstructed from ϕ with the help of postprocessing techniques. One of the most well-known methods is the Volume-of-Fluid (VOF) method [42, 54] in which case the indicator function ϕ can be interpreted as volume fraction which should have the discrete values 0 or 1 depending on the location of $\mathbf{x}$:

$$\phi(\mathbf{x}, t) = \begin{cases} 1, & \forall \mathbf{x} \in \Omega_1(t), \\ 0, & \forall \mathbf{x} \in \Omega_2(t). \end{cases} \tag{4.5}$$

The numerical drawback of this approach is that artificial diffusion smears out the (originally) discontinuous indicator function which arises from the solution of the discretized advection problems resulting in a boundary layer with $0 < \phi < 1$. Therefore, numerical schemes and locally adapted meshes have to be designed to address this boundary layer as thin as possible so that the corresponding error for reconstructing the free interface is reduced. Moreover, due to the steep gradients and the discontinuity of the indicator function, standard Galerkin schemes lead to unphysical oscillations which significantly deteriorate the accuracy or even lead to unphysical over- and undershoots. As a conclusion, the development of corresponding high-order monotone discretization schemes in combination with unstructured, locally refined meshes still belongs to the numerical challenges one has to solve.

As a successful alternative, the Level Set approach [43, 44, 53] has been established which represents the interface as zero isoline of a continuous indicator function ϕ which should be close to the distance with respect to the free interface

$$\phi(\mathbf{x}, t) = \begin{cases} \operatorname{dist}(\mathbf{x}, \Gamma), & \forall \mathbf{x} \in \Omega_1(t), \\ -\operatorname{dist}(\mathbf{x}, \Gamma), & \forall \mathbf{x} \in \Omega_2(t) \end{cases} \tag{4.6}$$

so that $\Gamma(t) = \{\mathbf{x} \in \Omega \mid \phi(\mathbf{x}, t) = 0\}$ holds. In contrast to the VOF approach, ϕ as a distance function is smooth and allows the calculation of a globally defined normal vector $\mathbf{n}$ towards the interface Γ and of the corresponding curvature via

$$\mathbf{n} = \frac{\nabla \phi}{|\nabla \phi|}, \qquad \kappa = -\nabla \cdot \mathbf{n} = -\nabla \cdot \left(\frac{\nabla \phi}{|\nabla \phi|} \right). \tag{4.7}$$

Here, special FEM techniques for gradient recovery can be used which allow highly accurate approximations of normals and curvature [56] which are necessary

for the direct evaluation of the surface tension force $\mathbf{f}_\Gamma = \kappa\sigma\delta(\phi)\mathbf{n}$, with $\delta(\phi)$ denoting the corresponding Dirac Delta function. Hence, the development and implementation of a typical Level Set approach consists of performing the following sequence of tasks:

- Discretization of the Level Set transport problem (4.4).
- Reinitialisation, resp., redistancing of the Level Set function.
- Additional correction so that mass and volume are preserved (if necessary).
- Calculation of normal vector fields (and curvature if needed) based on ϕ.
- Evaluation of the discontinuous fluid parameters $\rho(\phi)$, $\mu(\phi)$, and of $\mathbf{f}_\Gamma$, with or without reconstruction of Γ.

The above sequence of tasks involves a myriad of different possibilities and choices which inevitably lead to numerous differing solution approaches. This is evident from the rich collection of publications on Level Set methods which also demonstrates the high potential of these methods for a wide range of applications (see for instance the books by Osher [43] and Sethian [53]). However, the resulting quality of the solutions mainly depends on the underlying numerical and computational approaches, and one has to acknowledge the fact that most of the existing Level Set codes are still based on finite differences on uniform Cartesian meshes which are easy to implement. The drawback is that the computational cost typically is quite high since uniform mesh refinement has to be performed to resolve the necessary scales, particularly near the fluidic interfaces, but also due to complicated geometries with small-scale structures. Unstructured meshes are particularly well suited for such approaches which leads us to finite volume and finite element discretization methods which are the most prominent candidates for unstructured simulation approaches. Examples for corresponding approaches in the framework of VOF and Level Set methods can be found in [3, 7, 9, 16, 29, 38, 40, 49]. In many approaches, for example in the *Interface Proximity Adaption Method* of Barth and Sethian [3], the mesh is locally refined near the interface which also is quite easy to find if ϕ is a distance function [38].

Although finite element methods together with locally refined grids seem to possess a very advantageous behaviour for simulation of multiphase flow problems with free interfaces, most existing Level Set codes are still based on finite differences. It is only during the last ten years that FEM codes have been successfully applied for these special CFD problems ([46, 50, 57]; see also [15, 23, 40, 47, 56, 59]). However, there is still a huge potential for improvement if '*optimal*' modern discretization and solution techniques shall be adapted to the special characteristics of FEM-Level Set methods. In constructing a modern Level Set solver it is important to focus on unstructured meshes with local grid refinement strategies for highly nonstationary multiphase flow simulations, and make detailed studies for higher numerical stability. Additionally, stable and accurate discretization of the convective terms (for instance, VOF and Phase-Field methods show very steep gradients near the interface, similarly as Level Set approaches without redistancing), robust treatment of large density differences, and the handling of large surface tension σ also require special attention.

Summarizing the properties of FEM-Level Set techniques for multiphase flow problems, we can conclude the following (potentially) advantageous behaviour in comparison to interface tracking methods as well as VOF and Phase-Field approaches which motivates our recent and future work for the combination of FEM and Level Set methods:

- If the Level Set function satisfies the distance property, it is smooth so that even on highly uniform meshes qualitatively good results can be obtained. Local refinement around the interface will help to improve the accuracy, but in contrast to VOF and Phase-Field methods, which may lead to smeared interfaces due to numerical diffusion or to unphysical oscillations due to steep gradients, adaptive meshes are not necessary.
- Accurate FEM discretizations of a higher order can be adapted to the special characteristics of Level Set functions, that means higher smoothness because of the distance function properties.
- Accurate representations of the interface are provided, without explicit description, but even for complex geometrical changes, which is important for handling the surface tension term.
- Auxiliary quantities like normal vectors and curvature are provided, even globally, which is particularly advantageous for the Continuous Surface Force (CSF) [6] approach.

On the other hand, there are still several problems with Level Set approaches (and some of them are also valid for VOF and Phase-Field methods) which are numerically challenging and which are in the focus of our recent and also planned research activities:

- The standard Level Set formulation is not conservative which may lead to mass loss.
- Since reinitialisation is necessary to preserve the distance property, often highly expensive computational operations might be necessary, for instance via solving globally the Eikonal equation, or redistancing is based on 'cheaper' methods which however change the position and shape of the interface, again leading to mass loss.
- Due to the standard explicit treatment of surface tension, the time step size is restricted by the *capillary time step restriction*, that means the necessary time steps depend by purely numerical reasons on the size of surface tension and on the local mesh size.

In the following sections, we first of all describe the overall solution technique which is based on a discrete projection method which is followed by a discussion of the FEM discretization details, particularly regarding the Discontinuous Galerkin approach for treating the Level Set equation.

4.3 Discrete Projection Methods for Navier–Stokes Equations

In this section, we briefly review the '*Discrete Projection Method*' as a special variant of Multilevel Pressure Schur Complement (MPSC) approaches for the solution of incompressible flow problems, and we combine it with FEM discretization techniques. We will explain some characteristics of high-resolution FEM schemes as applied to incompressible flow problems and discuss the computational details regarding the efficient numerical solution of the resulting nonlinear and linear algebraic systems. Furthermore, we will discuss the coupling mechanisms between the 'basic' flow model (standard Navier–Stokes equations for velocity and pressure) and the scalar transport equations for the Level Set indicator function in our multiphase flow solver.

4.3.1 Discretization Techniques

For a better illustration, we consider first of all numerical solution techniques for the (single phase) incompressible Navier–Stokes equations,

$$\begin{aligned} \mathbf{u}_t - \nu\Delta\mathbf{u} + \mathbf{u}\cdot\nabla\mathbf{u} + \nabla p_\rho &= \mathbf{f}, \\ \nabla\cdot\mathbf{u} = 0, \quad \text{in } \Omega\times(0,T] \quad &\text{with } p_\rho = \frac{p}{\rho} \text{ and } \nu = \frac{\mu}{\rho}, \end{aligned} \tag{4.8}$$

for the given force $\mathbf{f}$ which might contain the surface tension. Moreover, boundary values are prescribed on the boundary $\partial\Omega$ as well as an initial condition at $t = 0$. Solving this problem numerically is still a considerable task in the case of long-time calculations and high Reynolds numbers, particularly in 3D and also in 2D if the time dynamics is complex. The common solution approach is a separate discretization in space and time. We first (semi-) discretize in time by one of the usual methods known from the treatment of ordinary differential equations, such as the Forward or Backward Euler-, the Crank–Nicolson- or Fractional-Step-θ–scheme, or others, and obtain a sequence of generalized stationary Navier-Stokes problems.

Basic θ-scheme Given $\mathbf{u}^n$ and $\Delta t = t_{n+1} - t_n$, then solve for $\mathbf{u} = \mathbf{u}^{n+1}$ and $p_\rho = p_\rho^{n+1}$

$$\frac{\mathbf{u}-\mathbf{u}^n}{\Delta t} + \theta[-\nu\Delta\mathbf{u} + \mathbf{u}\cdot\nabla\mathbf{u}] + \nabla p_\rho = \mathbf{g}^{n+1}, \qquad \nabla\cdot\mathbf{u} = 0, \quad \text{in } \Omega \tag{4.9}$$

with the right-hand side $\mathbf{g}^{n+1} := \theta\mathbf{f}^{n+1} + (1-\theta)\mathbf{f}^n - (1-\theta)[-\nu\Delta\mathbf{u}^n + \mathbf{u}^n\cdot\nabla\mathbf{u}^n]$.

In the following simulations, the parameter θ is chosen as $\theta = 1/2$, representing the Crank-Nicolson-scheme which is of second order. Alternatively, the Fractional-Step-θ-scheme [63], which uses three different values for θ and for the time step Δt at each time level, is another excellent candidate with slightly better robustness properties.

For the spatial discretization, we choose a finite element approach based on a suitable variational formulation. On the finite mesh $\mathcal{T}_h$ (3D hexahedral elements in our case) covering the domain Ω with the local mesh size h, one defines polynomial trial functions for velocity and pressure. These spaces H_h and L_h should lead to numerically stable approximations as $h \to 0$, i.e., they should satisfy the so-called *inf-sup* (LBB) condition [20]

$$\min_{q_h \in L_h} \max_{\mathbf{v}_h \in H_h} \frac{(q_h, \nabla \cdot \mathbf{v}_h)}{\|q_h\|_0 \, \|\nabla \mathbf{v}_h\|_0} \geq \gamma > 0 \tag{4.10}$$

with a mesh-independent constant γ. While the original FEATFLOW solvers are based on *rotated multilinear* nonconforming finite element functions for the velocity and piecewise constant pressure approximations, we recently extended the complete solver package to higher-order Stokes elements, namely conforming triquadratic ansatz functions for the velocity and linear pressure approximations (Q_2/P_1), which belong to the 'best' finite element pairs for laminar incompressible flow due to their accuracy and robustness. Since so far most of our numerical simulations have been performed for small up to moderate Reynolds numbers, the (nonlinear) convective operator was discretized using standard stabilization techniques only. Currently, we use edge-, resp., face-oriented FEM stabilization techniques [62] which can be easily realized for higher-order ansatz functions, too. Here, special jump terms of the gradient of the solution as well as of the test function have to be included into the weak formulation which leads to a consistent stabilization, for stationary as well as nonstationary configurations. It is planned to apply this technique in the case of higher Reynolds number flows, too, which will be a subject of our further studies for such multiphase flow problems. For an overview regarding such special FEM stabilization techniques, we refer to [45, 62] and particularly to [10] which contains corresponding results for the Q_2/P_1 approach, too.

4.3.2 Solution Techniques

Using the same notation $\mathbf{u}$ and p_ρ also for the coefficient vectors in the representation of the approximate solution, the discretized Navier-Stokes equations may be written as a coupled (nonlinear) algebraic system of the form: Given $\mathbf{u}^n$ and $\mathbf{f}$, compute $\mathbf{u} = \mathbf{u}^{n+1}$ and $p_\rho = p_\rho^{n+1}$ by solving

$$A\mathbf{u} + \Delta t B p_\rho = \mathbf{g}, \qquad B^T \mathbf{u} = 0, \tag{4.11}$$

where

$$\mathbf{g} = \left[M - \theta_1 \Delta t N\left(\mathbf{u}^n\right)\right]\mathbf{u}^n + \theta_2 \Delta t \mathbf{f}^{n+1} + \theta_3 \Delta t \mathbf{f}^n. \tag{4.12}$$

Here and in the following, we use the more compact form for the diffusive and advective part

$$N(\mathbf{v})\mathbf{u} := -\nu \Delta \mathbf{u} + \mathbf{v} \cdot \nabla \mathbf{u}, \tag{4.13}$$

while M is the (lumped) mass matrix [66], B is the discrete gradient operator, and $-B^T$ is the associated divergence operator. Furthermore,

$$A\mathbf{u} = \big[M - \theta \Delta t N(\mathbf{u})\big]\mathbf{u}, \quad N(\mathbf{u}) = K(\mathbf{u}) + \nu L, \tag{4.14}$$

where L is the discrete Laplacian and $K(\mathbf{u})$ is the nonlinear transport operator incorporating a certain amount of artificial diffusion due to some appropriate FEM stabilization as described before. The solution of nonlinear algebraic systems like (4.11) is a rather difficult task and many aspects, namely the treatment of the nonlinearity and of the incompressibility as well as the outer control of the couplings, need to be taken into account. Consequently, this leads to a great variety of incompressible flow solvers which are closely related to one another but exhibit considerable differences in terms of their stability, convergence, and efficiency. The Multilevel Pressure Schur Complement (MPSC) approach outlined below makes it possible to put many existing solution techniques into a common framework and to combine their advantages so as to obtain better run-time characteristics.

The fully discretized Navier-Stokes equations (4.11) as well as the linear subproblems to be solved within the outer iteration loop for a fixed-point defect correction or, with a similar structure, for a Newton-like method admit the following representation:

$$\begin{bmatrix} A & \Delta t B \\ B^T & 0 \end{bmatrix} \begin{bmatrix} \mathbf{u} \\ p_\rho \end{bmatrix} = \begin{bmatrix} \mathbf{g} \\ 0 \end{bmatrix}. \tag{4.15}$$

In general, we have $A = M + \beta N(\mathbf{u})$, with $\beta = -\theta \Delta t$ for time-dependent problems. If the operator A is nonsingular, the velocity can be formally expressed as

$$\mathbf{u} = A^{-1}(\mathbf{g} - \Delta t B p_\rho) \tag{4.16}$$

and plugged into the discretized continuity equation

$$B^T \mathbf{u} = 0 \tag{4.17}$$

which gives a scalar *Schur complement* equation for the pressure only

$$B^T A^{-1} B p_\rho = \frac{1}{\Delta t} B^T A^{-1} \mathbf{g}. \tag{4.18}$$

Thus, the coupled system (4.15) can be handled as follows:

1. Solve the Pressure Schur Complement (PSC) equation (4.18) for p_ρ.
2. Substitute p_ρ into the relation (4.16) and compute the velocity $\mathbf{u}$.

It is worth mentioning that the matrix A^{-1} is full and should not be assembled explicitly. Instead, an auxiliary problem is to be solved by a direct method or by inner iterations. For instance, the velocity update (4.16) is equivalent to the solution of the discretized momentum equation $A\mathbf{u} = \mathbf{g} - \Delta t B p_\rho$. Likewise, the matrix $S := B^T A^{-1} B$ is never generated in practice. Doing so would be prohibitively expensive in terms of CPU time and memory requirements. It is instructive to consider

a preconditioned Richardson method which yields the following **basic iteration** for the PSC equation:

$$p_\rho^{(l+1)} = p_\rho^{(l)} - C^{-1}\left[S p_\rho^{(l)} - \frac{1}{\Delta t} B^T A^{-1} \mathbf{g} \right], \quad l = 0, \ldots, L-1. \tag{4.19}$$

Here, C has to be chosen as a suitable preconditioner to S but being easier to 'invert' in an iterative way. The number of PSC cycles L can be fixed or chosen adaptively so as to achieve a prescribed tolerance for the residual. The basic idea behind the family of global MPSC schemes is the construction of globally defined additive preconditioners for the Schur complement operator $S = B^T A^{-1} B$. Recall that the matrix A has the structure

$$A := M + \beta K(\mathbf{u}) + \gamma L, \tag{4.20}$$

where $\beta = -\theta \Delta t$ and $\gamma = \nu\beta$. Unfortunately, even today it is still a very challenging task to construct a matrix $\tilde{A}$ and a preconditioner $C = B^T \tilde{A}^{-1} B$ that would be a sufficiently good approximation to all three components of A and S, respectively; particularly for the convective part with $K(\mathbf{u})$. Therefore, one may start with developing individual preconditioners for the reactive (M) and diffusive (L) part, while the convective (K) part is neglected by applying this special kind of operator splitting. In our case, the Reynolds numbers in the considered flow configurations are so far quite small, so that this approach can be justified, particularly if small time steps are used to resolve the complex dynamical behaviour. Therefore, the (lumped) mass matrix M proves to be a reasonable approximation to the complete operator A, so that our basic iteration (4.19) for the pressure Schur complement equation

$$p_\rho^{(l+1)} = p_\rho^{(l)} + \left[B^T M^{-1} B \right]^{-1} \frac{1}{\Delta t} B^T A^{-1} \left[\mathbf{g} - \Delta t B p_\rho^{(l)} \right] \tag{4.21}$$

can be interpreted and implemented as a *discrete projection scheme*, if $L = 1$, such as those proposed in [12, 22]. Here, the important step is that for the chosen Stokes element pair, Q_2/P_1, the matrix $P := B^T M^{-1} B$ can be explicitly built up relatively easily even in a domain decomposition framework due to the chosen discontinuous pressure. Then, the main algorithmic steps are as follows [60]:

Step 1. Solve the 'viscous Burgers' equation for $\tilde{\mathbf{u}}$

$$A\tilde{\mathbf{u}} = \mathbf{g} - \Delta t B p_\rho^{(l)}.$$

Step 2. Solve the discrete 'Pressure-Poisson' problem

$$P q_\rho = \frac{1}{\Delta t} B^T \tilde{\mathbf{u}}.$$

Step 3. Correct the pressure and the velocity

$$p_\rho^{(l+1)} = p_\rho^{(l)} + q_\rho, \qquad \mathbf{u} = \tilde{\mathbf{u}} - \Delta t M^{-1} B q_\rho.$$

In essence, the right-hand side of the momentum equation is assembled using the old pressure iterate, and the intermediate velocity $\tilde{\mathbf{u}}$ is projected onto the subspace of solenoidal functions so as to satisfy the constraint $B^T\mathbf{u} = 0$. Moreover, the matrix P corresponds to a mixed discretization of the Laplacian operator [22] so that this method is a discrete analogue of the classical projection schemes derived by Chorin ($p_\rho^{(0)} = 0$) and Van Kan ($p_\rho^{(0)} = p_\rho(t_n)$) via operator splitting for the continuous problem.

Next, we apply this special operator-splitting approach to the full multiphase flow system with a discontinuous density $\rho(\phi)$ and viscosity $\mu(\phi)$ distribution, that means

$$\rho(\phi)\left[\frac{\partial \mathbf{u}}{\partial t} + \mathbf{u}\cdot\nabla\mathbf{u}\right] - \nabla\cdot\left(\mu(\phi)\left[\nabla\mathbf{u} + (\nabla\mathbf{u})^T\right]\right) + \nabla p = \rho(\phi)\mathbf{g} + \mathbf{f}_{\Gamma,\sigma}(\phi), \tag{4.22}$$

$$\frac{\partial \phi}{\partial t} + \mathbf{u}\cdot\nabla\phi = 0, \qquad \nabla\cdot\mathbf{u} = 0. \tag{4.23}$$

After discretization in space and time, we obtain again a system of nonlinear algebraic equations which can be written in a matrix form as follows:

$$A_u\left(\mathbf{u}^{n+1}, \phi^{n+1}\right)\mathbf{u}^{n+1} + \Delta t\, F\left(\phi^{n+1}\right) + \Delta t\, B p^{n+1} = \mathbf{g}_u, \tag{4.24}$$

$$A_\phi\left(\mathbf{u}^{n+1}\right)\phi^{n+1} = g_\phi, \qquad B^T\mathbf{u}^{n+1} = 0. \tag{4.25}$$

Note that Eq. (4.24) in contrast to (4.11) and (4.14) is multiplied with $\rho(\phi)$, which gives rise to the modified operators M_ρ, $K_\rho(\mathbf{u})$, and L_μ. Here and below the superscript $n+1$ refers to the time level, while subscripts identify the origin of discrete operators (u for the momentum equation and ϕ for the Level Set equation); moreover, ρ and μ are evaluated w.r.t. the old time level t^n which makes this formulation semi-implicit. Note that we have the freedom of using different finite element approximations and discretization schemes for the velocity $\mathbf{u}$ and the indicator function ϕ, and the discrete problem (4.24)–(4.25) can be solved again in the framework of the discrete projection method. For relatively small time steps, this strategy works very well, and simulation software can be developed in a modular way making use of optimized multigrid solvers. Consequently, in the simplest case (just one outer iteration per time step), the sequence of algorithmic steps to be performed is as follows:

Step 1. Compute $\tilde{\mathbf{u}}$ from the momentum equation

$$A_u\left(\tilde{\mathbf{u}}, \phi^n\right)\tilde{\mathbf{u}} = \mathbf{g}_u - \Delta t\, F\left(\phi^n\right) - \Delta t\, B p^n.$$

Step 2. Solve the discrete Pressure-Poisson problem

$$P_\rho q = \frac{1}{\Delta t} B^T\tilde{\mathbf{u}} \quad \text{with } P_\rho := B^T M_\rho^{-1} B.$$

Step 3. Correct the pressure and the velocity

$$p^{n+1} = p^n + q, \qquad \mathbf{u}^{n+1} = \tilde{\mathbf{u}} - \Delta t M_\rho^{-1} B q.$$

Step 4. Solve the Level Set equation for ϕ

$$A_\phi\big(\mathbf{u}^{n+1}\big)\phi^{n+1} = g_\phi.$$

Due to the nonlinearity of the discretized convective terms, resp., of the reinitialisation step, iterative defect correction or Newton-like methods, resp., corrections via redistancing, must be invoked in Steps 1 and 4. However, due to the assumed relatively small time steps, such nonlinear iteration methods are not critical for the complete flow simulation.

4.4 The FEM-Level Set-dG(1) Approach

Our chosen Level Set approach is based on a first-order Discontinuous Galerkin discretization in space, dG(1)-FEM, that means on piecewise linear polynomials. In the following, we will discuss the corresponding techniques for the discretization of the advection equation, for the treatment of the surface tension force, and for the reinitialisation procedure.

4.4.1 Discontinuous Galerkin Upwinding for the Level Set Approach

There are several ways to approximate and solve Discontinuous Galerkin approximations for the Level Set function ϕ [11, 15, 36, 41]. The general form of the Level Set transport equation involving the normal front velocity can for instance be solved directly by using a Runge–Kutta dG-formulation for the Hamilton–Jacobi equations [27, 35]. The starting point to introduce our discretization of the Level Set transport equation is

$$\frac{\partial \phi}{\partial t} + \mathbf{u} \cdot \nabla \phi = 0 \tag{4.26}$$

with a given velocity field $\mathbf{u}$. In our case $\mathbf{u}$ is taken as the convective velocity from the Navier–Stokes solver and must accordingly be updated in each time step. We have $\mathbf{u} \cdot \mathbf{n} = u_n$, where $\mathbf{n}$ is the unit normal to the interface Γ according to (4.7). The Level Set equation (4.26) can thus be rewritten as

$$\frac{\partial \phi}{\partial t} + \nabla \cdot (\mathbf{u}\phi) = \phi \nabla \cdot \mathbf{u}. \tag{4.27}$$

The reformulated Level Set equation above is simply a linear convection or advection equation in conservative formulation with a source term on the right hand

side. We continue to rewriting it in weak form by introducing a triangulation, $\mathscr{M}_h$, of the domain Ω where $\mathscr{E}$ is an element $\mathscr{E} \in \mathscr{M}^h$. We are thus seeking an approximated solution in the following space

$$V_h = \left\{ v_h \in L^\infty(\Omega) : v_h|_{\mathscr{E}} \in V_h(\mathscr{E}), \forall \mathscr{E} \in \mathscr{M}^h \right\}.$$

Here, $V_h(\mathscr{E})$ denotes the local discrete test and trial spaces. The corresponding derivation follows by multiplying the equation (4.26) by a suitably chosen test function after which partial integration over each element $\mathscr{E}$ is performed. If the trial solution space is accordingly discretized as $\phi_h \in V_h(\mathscr{E})$, this results in

$$\int_{\mathscr{E}} v_h \frac{\partial \phi_h}{\partial t} dx = \int_{\mathscr{E}} \phi_h \mathbf{u} \cdot \nabla v_h dx - \int_{\partial \mathscr{E}} v_h \phi_h \mathbf{u} \cdot \mathbf{n}_{\mathscr{E}} ds + \int_{\mathscr{E}} v_h \phi_h \nabla \cdot \mathbf{u} dx,$$
$$\forall v_h \in V_h(\mathscr{E}), \tag{4.28}$$

where $\mathbf{n}_{\mathscr{E}}$ is the outward pointing unit normal belonging to the element $\mathscr{E}$. The fluxes on the internal boundaries are twofold defined since the underlying test and trial spaces are discontinuous. This is handled by replacing the outer flux in the last term of the right-hand side of Eq. (4.28) with a numerically upwinded flux, that is

$$\int_{\mathscr{E}} v_h \frac{\partial \phi_h}{\partial t} dx = \int_{\mathscr{E}} \phi_h \nabla \cdot (\mathbf{u} v_h) dx - \int_{\partial \mathscr{E}} v_h \phi_h^{up} \mathbf{u} \cdot \mathbf{n}_{\mathscr{E}} ds, \quad \forall v_h \in V_h(\mathscr{E}). \tag{4.29}$$

The upwinding flux is calculated as

$$\phi^{up} = \begin{cases} \phi^-, & \text{if } \mathbf{u} \cdot \mathbf{n}_{\mathscr{E}} \geq 0, \\ \phi^+, & \text{otherwise,} \end{cases}$$

where ϕ^- and ϕ^+ are defined as

$$\phi^- = \lim_{\epsilon \to 0^-} \phi(\mathbf{x} + \epsilon \mathbf{n}_\epsilon, t),$$
$$\phi^+ = \lim_{\epsilon \to 0^+} \phi(\mathbf{x} + \epsilon \mathbf{n}_\epsilon, t).$$

In other words this means that ϕ^{up} is the value of ϕ taken from an upwind element at an element interface.

In our approach, Eq. (4.29) is discretized in space by firstly constructing the triangulation $\mathscr{M}_h$ by subdivision in the hexahedral elements $\mathscr{E}$. Furthermore, both the test and trial function spaces, v_h and ϕ_h, are constructed by employing linear first-order polynomial basis functions on each element $\mathscr{E}$, the so-called dG(1) approach. These basis functions are completely determined by interior nodes of the element and are thus discontinuous at inter-element edges. Moreover, the discretization in time utilizes as before the standard second-order Crank–Nicolson scheme as described for instance in [61].

4.4.2 Treatment of Surface Tension Effects

Surface tension effects are taken into account through the following force balance at the interface Γ:

$$[\mathbf{u}]|_\Gamma = 0, \qquad \left[-p\mathbf{I} + \mu\left(\nabla\mathbf{u} + (\nabla\mathbf{u})^T\right)\right]\Big|_\Gamma \cdot \mathbf{n} = \sigma\kappa\mathbf{n}.$$

Here $\mathbf{n}$ is the unit normal at the interface pointing into Ω_1, $[\mathsf{A}]|_\Gamma = \mathsf{A}|_{\Omega_1\cap\Gamma} - \mathsf{A}|_{\Omega_2\cap\Gamma}$ denotes the jump of a quantity A across the interface, σ is the surface tension coefficient, and κ is the curvature of the interface Γ. The first condition implies continuity of the velocity across the interface, whereas the second describes the force balance on Γ. Two strategies are often used to handle the curvature term, either to rewrite it as a volume force, that means

$$\mathbf{f}_{st} = \sigma\kappa\mathbf{n}\delta(\Gamma, \mathbf{x}),$$

where $\delta(\Gamma, \mathbf{x})$ is the Dirac delta function localizing the surface tension forces to the interface, or to introduce the Laplace–Beltrami operator Δ_Γ on the interface, that means

$$\kappa\mathbf{n} = \Delta_\Gamma \,\mathrm{id}$$

and integrating the corresponding term in the weak formulation of the problem by parts [1, 17]. In the case of our current explicit treatment we get

$$(\mathbf{f}_{st}, \mathbf{v}) = \int_{\Gamma^n} \sigma\kappa^n\mathbf{n}^n \cdot \mathbf{v}\, d\Gamma, \tag{4.30}$$

where the superscript n denotes the previous time level. The extension of the surface integrals into volumetric ones can be obtained by the indicated incorporation of the Dirac Delta function $\delta = \delta(\Gamma, \mathbf{x})$, which has the value ∞ at the location of the interface, $\phi = 0$, and zero elsewhere, that means

$$(\mathbf{f}_{st}, \mathbf{v}) = \int_\Omega \sigma\kappa^n\mathbf{n}^n \cdot \mathbf{v}\delta\left(\Gamma^n\right) dx. \tag{4.31}$$

According to the applied CSF approach we approximate the Dirac Delta function δ by a continuous regularized one, which is a smooth function in the vicinity ϵ of the interface:

$$\delta(\phi) = \begin{cases} \phi < 0, & \max(0, \frac{1}{\epsilon} + \frac{1}{\epsilon^2}\phi), \\ \phi \geq 0, & \max(0, \frac{1}{\epsilon} - \frac{1}{\epsilon^2}\phi). \end{cases} \tag{4.32}$$

Since the interface normal $\mathbf{n}^n$ and curvature κ^n are higher order derivatives of the Level Set function ϕ^n, their distributions can be obtained by a combination of appropriate projection and gradient recovery techniques. Accordingly, the continuous (piecewise trilinear) interface normal $\mathbf{n}^n_{Q_1}$ is obtained by L_2-projection (and normalization) from the piecewise discontinuous P_1 space into the continuous Q_1 space.

Finally, the continuous approximation $\kappa^n_{Q_1}$ of the curvature κ^n is reconstructed via L_2-projection, too,

$$\int_\Omega \kappa^n_{Q_1} w \, dx = -\int_\Omega w \, \nabla \cdot \mathbf{n}^n_{Q_1} \, dx, \tag{4.33}$$

where w denotes the test functions from the conforming trilinear Q_1 space.

One of the remaining challenging problems is the *capillary time step restriction* which couples the time step size with the (local) mesh size h and $1/\sigma$ leading to very high computational cost due to such strict stability constraints. Beside the classical work by Bänsch, who developed a semi-implicit approach for front tracking, the FEM-Level Set approach by Hysing [28] is one of the very few attempts for interface capturing methods, which is in the focus of our future research on 3D multiphase flow problems. Very recently, an alternative method containing a survey on this problem and existing solution strategies was published by Sussmann [58]. However, it still has to be stated that the combination of adaptive Level Set or VOF methods on locally adapted meshes shows severe numerical problems if configurations with large surface tension shall be simulated in an accurate, robust, and efficient way. Moreover, the challenges further increase for non-Newtonian multiphase fluids, for instance for Power Law models ('shear thinning' [13]) or for viscoelastic fluids [68] which even for single-phase flows lead to huge problems for large Weissenberg numbers. Nevertheless, we are convinced that the described FEM-Level Set techniques have the potential to solve these challenging problems in future.

As a final comment, in the framework of variational formulations, the corresponding volume integral can be reduced to a boundary integral which serves as a natural boundary condition at the free interface [48, 56]. Moreover, if partial integration of the *Laplace-Beltrami* operator is applied in tangential direction of the interface [1, 2, 14, 18, 24, 37] then the calculation of the second derivatives of ϕ for the curvature can be omitted which can be used for very efficient evaluations of the surface tension force in combination with Level Set functions satisfying the distance property. This is in contrast to the usual finite difference approaches which require a less accurate *Continuum Surface Force* (CSF) approximation of the (singular) Delta function [6]. The above-mentioned alternative treatment of the surface tension force term is in the scope of our forthcoming studies.

4.4.3 Reinitialization Procedure for LS-dG(1)

For the accurate calculation of the normal vector and curvature, as defined in (4.7), and hence for the accurate position and shape of the dynamic interface, one has to take care that ϕ satisfies—at least near the interface Γ—the distance property which typically is achieved via appropriate postprocessing of a given numerical approximation $\tilde{\phi}$. Since the direct *reinitialisation* $\phi_i := \text{sign}(\tilde{\phi}_i)\,\text{dist}(\mathbf{x}_i, \Gamma)$ is very expensive, one way to do the corresponding corrections is to solve the so-called Eikonal equation $|\nabla\phi| = 1$ [30, 33] with boundary conditions $\phi = 0$ on $\Gamma = \{\mathbf{x} \in$

$\Omega \mid \tilde{\phi}(\mathbf{x}) = 0\}$. Typical methods are based on *fast marching* [53] or *fast sweeping* [69], while another approach is based on pseudo-timestepping for this nonlinear equation which leads to a Hamilton–Jacobi PDE:

$$\frac{\partial \phi}{\partial \tau} = \operatorname{sign}(\tilde{\phi})\big(1 - |\nabla \phi|\big), \quad \phi|_{\tau=0} = \tilde{\phi}. \tag{4.34}$$

Corresponding numerical approaches exploit that this problem can be written as a (nonlinear) transport equation

$$\frac{\partial \phi}{\partial \tau} + \mathbf{w} \cdot \nabla \phi = \operatorname{sign}(\tilde{\phi}), \quad \text{with } \mathbf{w} = \operatorname{sign}(\tilde{\phi}) \frac{\nabla \phi}{|\nabla \phi|}. \tag{4.35}$$

By stability reasons, the (discontinuous) sign function is typically replaced by a smoothed approximation which may lead to loss of accuracy and shift of the free interface. In the framework of FEM, the *interface local projection* of Parolini [47] helps, particularly for piecewise linear functions leading to a constant gradient vector, which combines the advantages of direct and PDE-based reinitialisation. Then, the correction of $\tilde{\phi}$ mostly consists of three steps:

1. In mesh cells which contain the free boundary Γ, an exact reconstruction via (piecewise constant) gradient is applied.
2. Use a L_2 projection to obtain the best approximation of ϕ near Γ.
3. Outside of the 'surface domain' Ω_{int}, solve the equation (4.35) using the already calculated values of ϕ at the boundary of Ω_{int} as Dirichlet boundary conditions.

According to our implementation, the reinitialization of the Level Set distribution is based on the advantages offered by the Discontinuous Galerkin Finite Element Method dG(1). This particularly means that we perform segregated reinitialization procedures on different groups of elements. The identified groups are as follows:

- Elements intersected by the interface, we denote them by $\mathscr{E} \subset \mathscr{M}^0$.
- A few layers of elements in the positive direction ($\phi > 0$) from the interface, $\mathscr{E} \subset \mathscr{M}^+$.
- A few layers of elements in the negative direction ($\phi < 0$) from the interface, $\mathscr{E} \subset \mathscr{M}^-$.
- The rest of the domain, these are the elements $\mathscr{E} \subset \mathscr{M}^\infty$.

Such a segregated approach enables us to get rid of the discontinuity that the sign function $S(\phi)$ exhibits at elements intersected by the interface. Moreover, it reduces the computational overhead since the PDEs are computed in a reduced computational domain only. Summarizing, the developed algorithm for the reinitialization is as follows:

Step 1. Direct reinitialization for $\mathscr{E} \subset \mathscr{M}^0$:

$$\phi^n \overset{|\nabla \phi|=1}{\longrightarrow} \phi^{n+1}.$$

Step 2. PDE-based solution for $\mathscr{E} \subset \mathscr{M}^+$ with

$$\frac{\partial \phi}{\partial \tau} + \mathbf{n} \cdot \nabla \phi = +1.$$

Step 3. PDE-based solution for $\mathscr{E} \subset \mathscr{M}^-$ with

$$\frac{\partial \phi}{\partial \tau} - \mathbf{n} \cdot \nabla \phi = -1.$$

Step 4. Prescription of far field values for $\mathscr{E} \subset \mathscr{M}^\infty$: $\phi_{\mathrm{RI}}^{n+1} = \phi^\infty$.

Here

$$\mathbf{n} := \mathbf{n}^n = \frac{\nabla \phi^n}{|\nabla \phi^n|}.$$

The coupling between the individual groups of elements is achieved by imposing of boundary conditions from $\mathscr{E} \subset \mathscr{M}^0$ for the PDE-based reinitialization which is treated via the Fictitious Boundary Method approach [39]. One has to keep in mind that the discontinuous sign function does not cause a problem in Steps 2 and 3 since the discontinuity has been treated already in Step 1. Additionally, the Level Set function can be corrected due to mass loss which typically is performed by adding an appropriate constant c_ϕ so that the total volume of both phases remains constant [56]. Moreover, further improvements can be obtained via high-order discretization and grid adaptivity [11] which is a subject of ongoing research.

4.5 Numerical Simulations

This section contains several numerical studies for validating and evaluating the methodology described in the previous sections.

4.5.1 Single-Phase Flow Around a Cylinder

The first incompressible flow problem to be dealt with, particularly to demonstrate the accuracy of the high-order Q_2/P_1 approach, is the well-known benchmark *Flow around cylinder* developed in 1995 for the priority research program "Flow simulation on high-performance computers" under the auspices of DFG, the German Research Association [64]. This project was intended to facilitate the evaluation of various numerical algorithms for the incompressible Navier-Stokes equations in the laminar flow regime. A quantitative comparison of simulation results is possible on the basis of relevant flow characteristics such as pressure values as well as drag and lift coefficients, for which sufficiently accurate reference values are available (see also: www.featflow.de/en/benchmarks/ff_benchmarks.html).

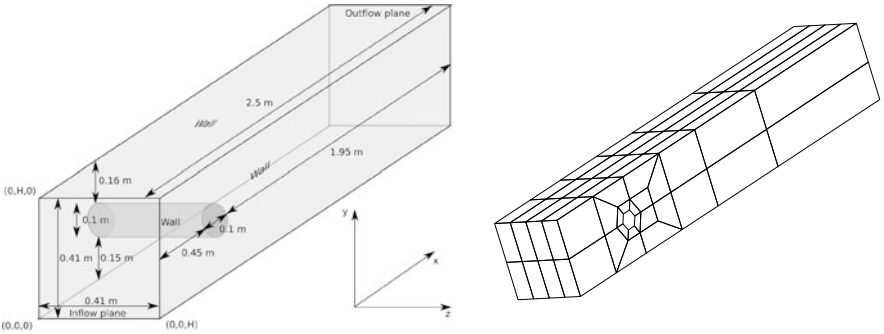

Fig. 4.2 Geometry and a coarse mesh for the 'Flow around cylinder' benchmark

Table 4.1 Mesh convergence results (levels 2 to 6) in terms of drag, lift, and pressure difference for the 'DFG Flow around cylinder problem' at $Re = 20$. Comparison of our results with reference results [5, 32]. ΔP refers to the pressure difference (front/back) on the cylinder and C_D and C_L are the normalized ($\frac{1}{2}\rho U_{\text{mean}}^2 L_{\text{cyl}} D_{\text{cyl}}$) drag and lift coefficients

Level	ΔP	C_D	C_L	NEL	NDOF($\mathbf{u}$, p)
2	0.171956	6.01954	0.012316	768	21,560
3	0.171553	6.13973	0.009569	6,144	199,200
4	0.171156	6.17433	0.009381	49,152	1,482,816
5	0.171031	6.18261	0.009387	393,216	11,432,064
6	0.171022	6.18465	0.009397	3,145,728	89,760,016
Authors	Reference values				
Braack [5]	0.171007	6.18533	0.009401	1,000,000	40,000,000
John [32]	0.170779	6.18533	0.009401	2,000,000	55,000,000

Here, we consider the steady incompressible flow around a cylinder with circular cross-section (see Fig. 4.2). An in-depth description of the geometrical details and boundary conditions can be found in [4, 64] which contain all relevant information regarding this benchmark configuration. The flow at $Re = 20$ is actually dominated by diffusion and could be simulated by the standard Galerkin method without any extra stabilization. The corresponding results are shown in Table 4.1 and demonstrate the high quality of the Q_2/P_1 approach compared to quasi-reference values from the literature [5, 32].

4.5.2 Two-Phase Flow of a Rising Bubble

The rising bubble configurations described in this section were chosen as the ones established by the numerical studies of van Sint Annaland et al. [54] in order to

Table 4.2 Resulting the Reynolds numbers obtained for the different configurations. The subscripts E and S stand for empirical and simulational reference values from Grace [8] and van Sint Annaland [54], respectively. The last four values refer to our simulation results obtained on the meshes A and B and on the refinement levels 2, 3, and 4

Case	Shape	Mo	Eo	Re_E	Re_S	Re_{mAl2}	Re_{mAl3}	Re_{mBl3}	Re_{mBl4}
B	Ellipsoidal	0.100	9.71	4.6	4.3	5.50	5.50	5.60	5.60
C	Skirted	0.971	97.1	20.0	18.0	17.7	18.0	18.0	18.0
D	Dimpled	1000	97.1	1.5	1.7	2.00	2.03	2.03	2.03

validate the implementation of our Level Set approach. According to the mentioned studies, the cases B, C, and D were analysed which results in a considerable deformation of the initial bubble. The ratios of physical properties ($\rho_g : \rho_l$ and $\mu_g : \mu_l$) of the present phases were set to (1 : 100). The ratios of the bubble diameter, d_b, with respect to the domain sizes, a_x, a_y, a_z, were $(d_b : a_x : a_y : a_z) = (3 : 10 : 10 : 20)$. The values of the interfacial tension coefficient σ_{gl} and gravitational acceleration g_z for the simulations were set based on the characteristic Eötvös and Morton numbers defined as in [8]:

$$\mathrm{Mo} = \frac{g_z \mu_l^4 \Delta\rho_{gl}}{\rho_l^2 \sigma_{gl}^3}, \qquad \mathrm{Eo} = \frac{g_z \Delta\rho_{gl} d_b^2}{\sigma_{gl}}. \tag{4.36}$$

As a result of the given settings the bubbles deform to a final shape and they reach an equilibrium rising velocity, v_∞, characterized by the Reynolds number defined as in [8]:

$$Re = \frac{\rho_l v_\infty d_b}{\mu_l}. \tag{4.37}$$

Since the Level Set approach by its nature does not preserve the mass of the individual phases, certain mass correction techniques were incorporated to prevent artificial '*mass transformation*' from one phase to another. To this end we adopted a simple but efficient method proposed by Smolianski [56] which elevates the level set function at every time step with a limited constant $\min(d_\varepsilon, \max(-d_\varepsilon, c_\phi))$, where d_ε is related to the characteristic element size and c_ϕ is a value enforcing absolute mass conservation. According to our experience setting d_ε to 3 % of the characteristic element size already prevents the occurrence of permanent mass loss.

In order to achieve mesh-independent simulation results in terms of bubble shape and terminal rising velocity, we performed the simulations on two sets of meshes of two consequent levels of refinements (mesh A with refinement level 2, 3 and mesh B refinement level 3, 4). As it can be seen from Fig. 4.3, which displays the equilibrium bubble shapes centered with respect to their center of mass, the bubble shapes converge fairly well with increasing mesh resolution, especially in cases B and D. The terminal rise velocities compared with the empirical predictions of Grace [8] and numerical predictions of van Sint Annaland [54] are given in Table 4.2. Despite the mesh-independent properties of the obtained results, the comparison of the

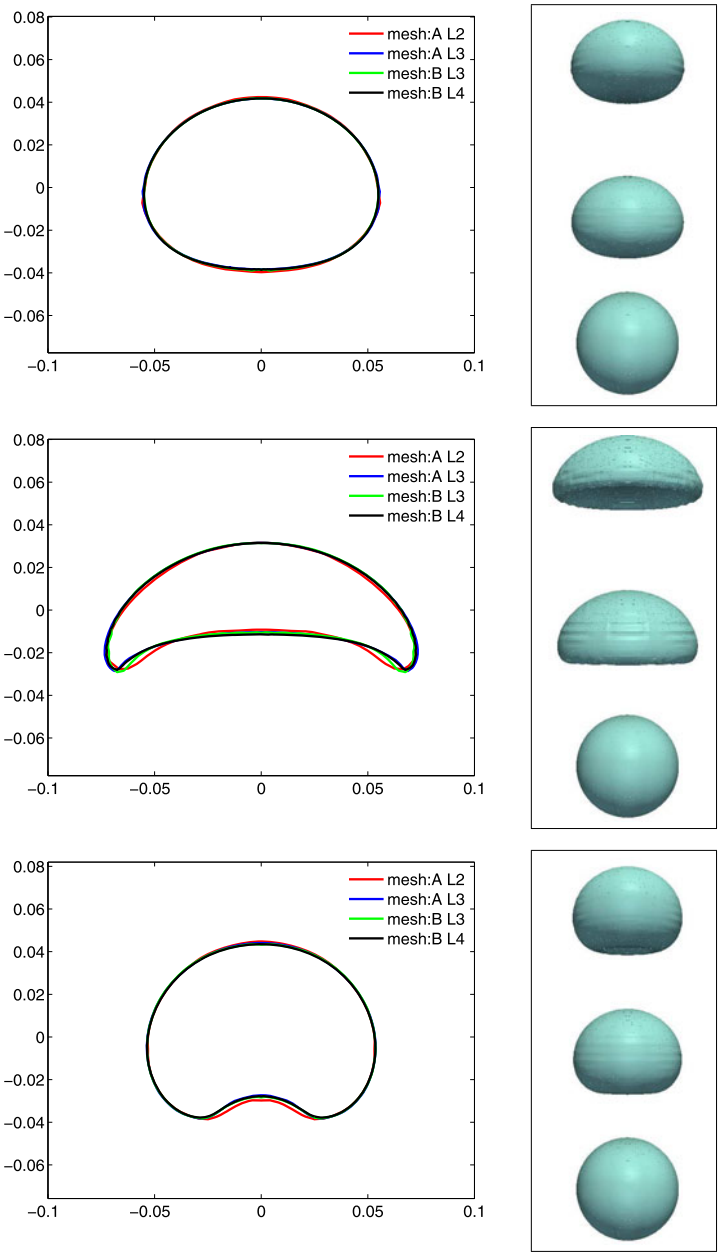

Fig. 4.3 *Left*: Cutplanes of continuous reconstructions of the interphase for the equilibrium bubble shapes. *Right*: Time evolution of the bubble shapes (from bottom to top). The cases are organized as: *Top*—case B—Eo = 9.71, Mo = 0.1; *Middle*—case C—Eo = 97.1, Mo = 0.971; *Bottom*—case D—Eo = 97.1, Mo = 1000

terminal rise velocities shows a weaker correlation of our results with the empirical predictions of Grace than it was the case in van Sint Annaland's computational studies. This contradiction leaves behind the challenges for further numerical analysis, possibly leading to a benchmark problem to which other researchers will also be welcome to contribute, as was the case with the well-known 2D rising bubble problem [31].

4.5.3 Droplet Dripping Simulation

The corresponding experimental setup involves a two-phase problem consisting of a glucose-water mixture (as a continuous phase) and silicon oil (as a dispersed phase). The measurements are restricted to the so-called dripping mode. This mode is characterized by relatively low volumetric flow rates and by the fact that the droplets are generated in the near vicinity of the capillary so that the stream length is comparable with the size of the generated droplets. Since the temperature is kept at a constant value during the whole experiment, all physical properties of the present phases are constant. The experimental measurements were realized (by the group of Prof. Walzel, BCI, TU Dortmund) to obtain statistically averaged quantities such as droplet size, droplet generation frequency and stream length. These experimentally measured quantities are compared with our subsequent simulation results.

The basic units used to define the derived quantities are the following ones:

$$[\text{length}] = \text{dm}, \qquad [\text{time}] = \text{s}, \qquad [\text{mass}] = \text{kg}.$$

The list of physical quantities is as follows (Fig. 4.4):

$$g_z = -9.81\ \text{m}\,\text{s}^{-2} = -98.1\ \text{dm}\,\text{s}^{-2},$$
$$\sigma = 0.034\ \text{N}\,\text{m}^{-1} = 0.034\ \text{kg}\,\text{s}^{-2},$$
$$\rho_C = 1340\ \text{kg}\,\text{m}^{-3} = 1.34\ \text{kg}\,\text{dm}^{-3},$$
$$\rho_D = 970\ \text{kg}\,\text{m}^{-3} = 0.97\ \text{kg}\,\text{dm}^{-3},$$
$$\mu = \mu_C = \mu_D = 500\ \text{mPa}\,\text{s} = 0.050\ \text{kg}\,\text{dm}\,\text{s}^{-1}.$$

The list of geometrical parameters reads:

$[\text{domain size}] = [-0.15 : 0.15] \times [-0.15 : 0.15] \times [0.0 : 1.2]\ \text{dm}^3$,
$[\text{inner capillary radius}] = R_1 = 0.015$ dm,
$[\text{outer capillary radius}] = R_2 = 0.030$ dm,
$[\text{primary phase inflow radius}] = R_3 = 0.15$ dm.

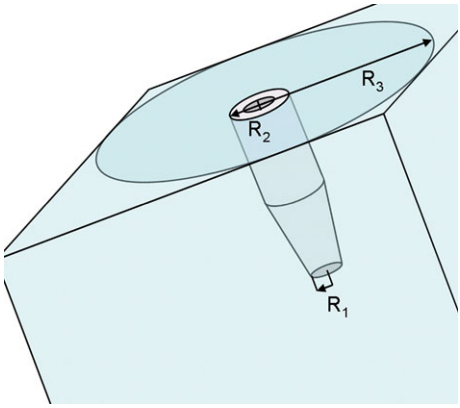

Fig. 4.4 A sketch of the benchmark domain

The boundary conditions imposed on the inflow velocity are the following:

$$w = \begin{cases} a_2(R_1 - r)(R_1 + r) & \text{if } 0 < r < R_1 \text{ (a dispersed phase)}, \\ a_1(R_3 - r)(r - R_2) & \text{if } R_2 < r < R_3 \text{ (a continuous phase)}, \\ 0 & \text{otherwise.} \end{cases}$$

The parameters a_1 and a_2 are defined to achieve the required volumetric flow rates:

$$\dot{V}_C = \int_{R_2}^{R_3} \left(2\pi r a_1 (R_3 - r)(r - R_2)\right) dr$$

$$= -2\pi a_1 \left[\frac{r^4}{4} - (R_2 + R_3)\frac{r^3}{3} + R_2 R_3 \frac{r^2}{2}\right]_{R_2}^{R_3} = \frac{\pi a_1}{6}(R_2 + R_3)(R_3 - R_2)^3.$$

$$\dot{V}_D = \int_0^{R_1} \left(2\pi r a_2 (R_1 - r)(R_1 + r)\right) dr = 2\pi a_2 \left[\frac{R_1^2 r^2}{2} - \frac{r^4}{4}\right]_0^{R_1} = \frac{\pi a_2}{2} R_1^4.$$

The volumetric flow rates for the simulations are set to:

$$\dot{V}_C = 99.04 \text{ ml min}^{-1} = 99.04 \text{ cm}^3 \text{ min}^{-1} = 99.04 \frac{10^{-3} \text{ dm}^3}{60 \text{ s}}$$

$$= 1.65 \times 10^{-3} \text{ dm}^3 \text{ s}^{-1},$$

$$\dot{V}_D = 3.64 \text{ ml min}^{-1} = 3.64 \text{ cm}^3 \text{ min}^{-1} = 3.64 \frac{10^{-3} \text{ dm}^3}{60 \text{ s}}$$

$$= 6.07 \times 10^{-5} \text{ dm}^3 \text{ s}^{-1},$$

which is guaranteed by setting $a_1 = 10.14 \text{ dm}^{-1} \text{ s}^{-1}$ and $a_2 = 763.7 \text{ dm}^{-1} \text{ s}^{-1}$.

The resulting process leads to a pseudo-steady state, where the droplet separation happens according to the so-called dripping mode. The frequency of the given mode is $f = 0.60 \text{ Hz}$ (cca $0.58 \text{ Hz}^{\text{exp}}$), which produces droplets of size $d = 0.058 \text{ dm}$ (cca

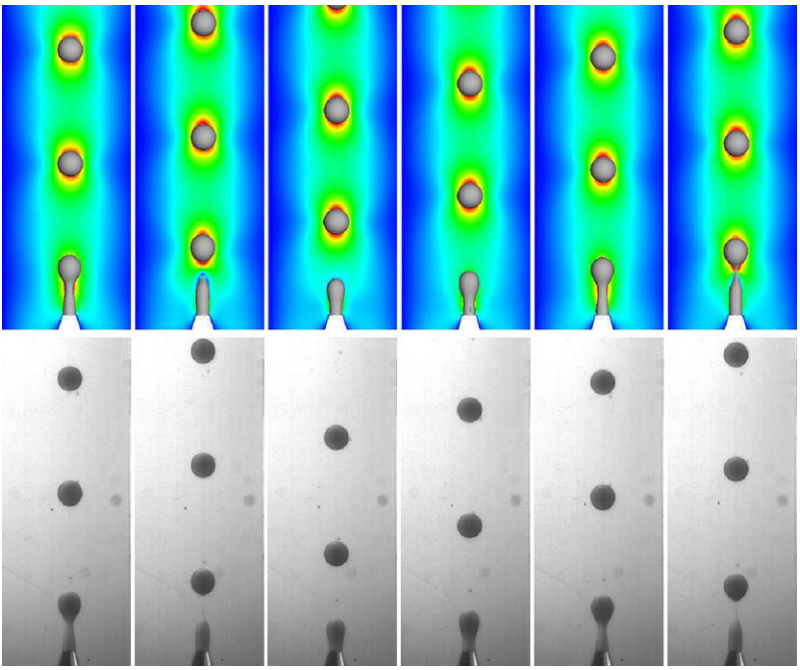

Fig. 4.5 A sequence of one droplet separation compared with experimental measurements

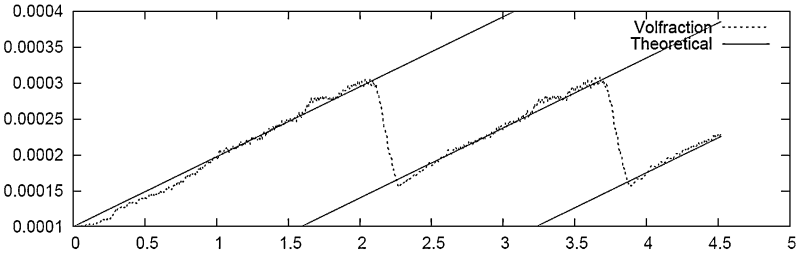

Fig. 4.6 Evolution of the volume of the secondary phase. Theoretical lines are characterized by the slope $q = 6.07 \times 10^{-5}\ \mathrm{dm^3\,s^{-1}}$

$0.062\,\mathrm{dm}^{\mathrm{exp}}$). The maximum stream length during the process is $L = 0.102\,\mathrm{dm}$ (cca $0.122\,\mathrm{dm}^{\mathrm{exp}}$). The snapshots of one full droplet generation compared with experimental measurements are given in Fig. 4.5. The time evolution of the volume of the secondary phase is given in Fig. 4.6. As it can be seen, the increase of the volume of the dispersed phase follows the theoretically expected trend in a reasonable way despite the fact that the mass correction technique (previously described in Sect. 4.5.2) was not activated.

4.6 Summary

In this contribution, we have shown that the realization of a new FEM-Level Set approach in the framework of Discontinuous Galerkin Finite Elements together with special PDE-based reinitialization techniques leads to very efficient simulation tools for modelling multiphase flow problems. The implemented parallel 3D multiphase flow solver has been validated in the case of the rising bubble and for the droplet dripping problem. A detailed description of these problems together with the obtained results—which are accurate and in fairly good agreement with the corresponding empirical data—are left in the form of a benchmark proposal for the engineering community.

Acknowledgements The authors would like to thank the German Research Foundation (DFG) for partially supporting the work under the grants Sonderforschungsbereich SFB708 (TP B7) and SPP 1423 (Tu102/32-1) and the group of Prof. Walzel at TU Dortmund for the experimental measurements supported by the grants Paketantrag PAK178 (Tu102/27-1, Ku1530/5-1).

References

1. Bänsch E (1998) Numerical methods for the instationary Navier-Stokes equations with a free capillary surface. Habil. thesis, Universität Freiburg, Freiburg
2. Bänsch E (2001) Finite element discretization of the Navier-Stokes equations with a free capillary surface. Numer Math 88(2):203–235. doi:10.1007/s002110000225
3. Barth TJ, Sethian JA (1998) Numerical schemes for the Hamilton-Jacobi and level set equations on triangulated domains. J Comput Phys 145(1):1–40
4. Bayraktar E, Mierka O, Turek S (2011) Benchmark computations of 3D laminar flow around a cylinder with CFX, OpenFOAM and FEATFLOW. Internat J Comput Sci Engrg. To appear. Also available as: Ergebnisberichte des Instituts für Angewandte Mathematik Nummer 433, Fakultät für Mathematik, TU, Dortmund
5. Braack M, Richter T (2006) Solutions of 3D Navier-Stokes benchmark problems with adaptive finite elements. Comput Fluids 35(4):372–392
6. Brackbill JU, Kothe DB, Zemach C (1992) A continuum method for modeling surface tension. J Comput Phys 100(2):335–354
7. Chen T, Minev PD, Nandakumar K (2004) A projection scheme for incompressible multiphase flow using adaptive Eulerian grid. Int J Numer Methods Fluids 45(1):1–19. doi:10.1002/fld.591
8. Clift R, Grace JR, Weber ME (2005) Bubbles, drops and particles. Dover, New York
9. Croce R, Griebel M, Schweitzer MA (2010) Numerical simulation of bubble and droplet deformation by a level set approach with surface tension in three dimensions. Int J Numer Methods Fluids 62(9):963–993. doi:10.1002/fld.2051
10. Damanik H (2011) Monolithic FEM techniques for viscoelastic fluids. PhD thesis, TU Dortmund, Dortmund
11. Di Pietro DA, Lo Forte S, Parolini N (2006) Mass preserving finite element implementations of the level set method. Appl Numer Math 56(9):1179–1195. doi:10.1016/j.apnum.2006.03.003
12. Donea J, Giuliani S, Laval H, Quartapelle L (1982) Finite element solution of the unsteady Navier-Stokes equations by a fractional step method. Comput Methods Appl Mech Eng 30(1):53–73
13. Dravid V, Songsermpong S, Xue ZJ, Corvalan CM, Sojka PE (2006) Two-dimensional modeling of the effects of insoluble surfactant on the breakup of a liquid filament. Chem Eng Sci 61(11):3577–3585

14. Dziuk G (1991) An algorithm for evolutionary surfaces. Numer Math 58(6):603–611
15. Farthing MW, Kees CE (2008) Implementation of discontinuous Galerkin methods for the level set equation on unstructured meshes. Technical note CHETN-XIII-2, U.S. Army Engineer Research and Development Center
16. Frolkovič P, Logashenko D, Wittum G (2008) Flux-based level set method for two-phase flow. Towards pure finite-volume discretization of incompressible two-phase flow using a level set formulation. In: Finite volumes for complex applications V. Wiley-ISTE, New York, pp 415–422
17. Ganesan S (2006) Finite element methods on moving meshes for free surface and interface flows. Published as a book by docupoint-Verlag, Magdeburg, 2006. PhD thesis, Otto-von-Guericke-Universität, Magdeburg
18. Ganesan S, Matthies G, Tobiska L (2007) On spurious velocities in incompressible flow problems with interfaces. Comput Methods Appl Mech Eng 196(7):1193–1202. doi:10.1016/j.cma.2006.08.018
19. Ganesan S, Tobiska L (2006) Computations on flows with interfaces using arbitrary Lagrangian Eulerian method. In: European conference on computational fluid dynamics ECCOMAS CFD 2006. TU Delft
20. Girault V, Raviart P-A (1986) Finite element methods for Navier-Stokes equations. Springer, Berlin
21. Glimm J, Grove JW, Li XL, Shyue K-M, Zeng Y, Zhang Q (1998) Three-dimensional front tracking. SIAM J Sci Comput 19(3):703–727
22. Gresho PM, Chan ST, Lee RL, Upson CD (1984) A modified finite element method for solving the time-dependent, incompressible Navier-Stokes equations. Part 1: Theory. Int J Numer Methods Fluids 4(6):557–598
23. Groß S, Reichelt V, Reusken A (2006) A finite element based level set method for two-phase incompressible flows. Comput Vis Sci 9(4):239–257
24. Groß S, Reusken A (2007) Finite element discretization error analysis of a surface tension force in two-phase incompressible flows. SIAM J Numer Anal 45(4):1679–1700
25. Hansbo A, Hansbo P (2002) An unfitted finite element method, based on Nitsche's method, for elliptic interface problems. Comput Methods Appl Mech Eng 191(47–48):5537–5552
26. Houzeaux G, Codina R (2003) A Chimera method based on a Dirichlet/Neumann(Robin) coupling for the Navier-Stokes equations. Comput Methods Appl Mech Eng 192(31–32):3343–3377
27. Hu C, Shu C-W (1999) A discontinuous Galerkin finite element method for Hamilton-Jacobi equations. SIAM J Sci Comput 21(2):666–690
28. Hysing S (2006) A new implicit surface tension implementation for interfacial flows. Int J Numer Methods Fluids 51(6):659–672. doi:10.1002/fld.1147
29. Hysing S (2007) Numerical simulation of immiscible fluids with FEM level set techniques. PhD thesis, Universität Dortmund, Dortmund
30. Hysing S, Turek S (2005) The Eikonal equation: numerical efficiency vs. algorithmic complexity on quadrilateral grids. In: Proceedings of algorithmy, Bratislava, Slovak University of Bratislava, pp 22–31
31. Hysing S, Turek S, Kuzmin D, Parolini N, Burman E, Ganesan S, Tobiska L (2009) Quantitative benchmark computations of two-dimensional bubble dynamics. Int J Numer Methods Fluids 60(11):1259–1288. doi:10.1002/fld.1934
32. John V (2006) On the efficiency of linearization schemes and coupled multigrid methods in the simulation of a 3D flow around a cylinder. Int J Numer Methods Fluids 50(7):845–862. doi:10.1002/fld.1080
33. Jones MW, Bærentzen JA, Sramek M (2006) 3D distance fields: a survey of techniques and applications. IEEE Trans Vis Comput Graph 12(4):581–599
34. Kuzmin D, Turek S (2004) High-resolution FEM-TVD schemes based on a fully multidimensional flux limiter. J Comput Phys 198(1):131–158. doi:10.1016/j.jcp.2004.01.015
35. Li F, Shu C-W (2005) Reinterpretation and simplified implementation of a discontinuous Galerkin method for Hamilton-Jacobi equations. Appl Math Lett 18(11):1204–1209

36. Marchandise E, Remacle J-F (2006) A stabilized finite element method using a discontinuous level set approach for solving two phase incompressible flows. J Comput Phys 219(2):780–800
37. Matthies G (2002) Finite element methods for free boundary value problems with capillary surfaces. PhD thesis, Otto-von-Guericke-Universität, Magdeburg. Published as a book by Shaker Verlag, Aachen, 2002
38. Minev PD, Chen T, Nandakumar K (2003) A finite element technique for multifluid incompressible flow using Eulerian grids. J Comput Phys 187(1):255–273
39. Münster R, Mierka O, Turek S (2012) Finite element-fictitious boundary methods (FEM-FBM) for 3D particulate flow. Int J Numer Methods Fluids 69(2):294–313. doi:10.1002/fld.2558
40. Nagrath S, Jansen KE, Lahey RT (2005) Computation of incompressible bubble dynamics with a stabilized finite element level set method. Comput Methods Appl Mech Eng 194(42–44):4565–4587
41. Nguyen V-T, Peraire J, Khoo BC, Persson P-O (2010) A discontinuous Galerkin front tracking method for two-phase flows with surface tension. Comput Fluids 39(1):1–14. doi:10.1016/j.compfluid.2009.06.007
42. Nichols BD, Hirt CW (1975) Methods for calculating multidimensional, transient free surface flows past bodies. In: Proc. of the first international conf. on numerical ship hydrodynamics, Gaithersburg, MD
43. Osher S, Fedkiw R (2003) Level set methods and dynamic implicit surfaces. Springer, Berlin
44. Osher S, Sethian JA (1988) Fronts propagating with curvature-dependent speed: algorithms based on Hamilton-Jacobi formulations. J Comput Phys 79(1):12–49. doi:10.1016/0021-9991(88)90002-2
45. Ouazzi A (2006) Finite element simulation of nonlinear fluids with application to granular material and powder. PhD thesis, Universität Dortmund, Dortmund, 2005. Published as a book by Shaker Verlag, Aachen
46. Owen HC (2009) A finite element model for free surface and two fluid flows on fixed meshes. PhD thesis, Universitat Politècnica de Catalunya, Barcelona
47. Parolini N (2004) Computational fluid dynamics for naval engineering problems. PhD thesis, École Polytechnique Fédérale de Lausanne (EPFL)
48. Parolini N, Burman E (2005) A finite element level set method for viscous free-surface flows. In: Applied and industrial mathematics in Italy, proceedings of SIMAI 2004. World Scientific, Singapore, pp 416–427
49. Preußer T, Rumpf M (2002) A level set method for anisotropic geometric diffusion in 3D image processing. SIAM J Appl Math 62(5):1772–1793
50. Quecedo M, Pastor M (2001) Application of the level set method to the finite element solution of two-phase flows. Int J Numer Methods Eng 50(3):645–663
51. Ramaswamy B, Kawahara M (2005) Arbitrary Lagrangian-Eulerianc finite element method for unsteady, convective, incompressible viscous free surface fluid flow. Int J Numer Methods Fluids 7(10):1053–1075
52. Scardovelli R, Zaleski S (1999) Direct numerical simulation of free-surface and interfacial flow. Annu Rev Fluid Mech 31:567–603. doi:10.1146/annurev.fluid.31.1.567
53. Sethian JA (1999) Level set methods and fast marching methods: evolving interphases in computational geometry, fluid mechanics, computer vision, and materials science 2nd ed. Cambridge University Press, Cambridge
54. van Sint Annaland M, Deen NG, Kuipers JAM (2005) Numerical simulation of gas bubbles behaviour using a three-dimensional volume of fluid method. Chem Eng Sci 60(11):2999–3011. doi:10.1016/j.ces.2005.01.031
55. van Sint Annaland M, Dijkhuizen W, Deen NG, Kuipers JAM (2006) Numerical simulation of behavior of gas bubbles using a 3-D front-tracking method. AIChE J 52(1):99–110. doi:10.1002/aic.10607
56. Smolianski A (2001) Numerical modeling of two-fluid interfacial flows. PhD thesis, University of Jyväskylä

57. Smolianski A (2005) Finite-element/level-set/operator-splitting (FELSOS) approach for computing two-fluid unsteady flows with free moving interfaces. Int J Numer Methods Fluids 48(3):231–269
58. Sussman M, Ohta M (2009) A stable and efficient method for treating surface tension in incompressible two-phase flow. SIAM J Sci Comput 31(4):2447–2471
59. Tornberg A-K (2000) Interface tracking methods with applications to multiphase flows. PhD thesis, Royal Institute of Technology (KTH)
60. Turek S (1997) On discrete projection methods for the incompressible Navier-Stokes equations: an algorithmical approach. Comput Methods Appl Mech Eng 143(3–4):271–288. doi:10.1016/S0045-7825(96)01155-3
61. Turek S (1999) Efficient solvers for incompressible flow problems: An algorithmic and computational approach. Lecture notes in computational science and engineering, vol 6. Springer, Berlin
62. Turek S, Ouazzi A (2007) Unified edge-oriented stabilization of nonconforming FEM for incompressible flow problems: numerical investigations. J Numer Math 15(4):299–322
63. Turek S, Rivkind L, Hron J, Glowinski R (2006) Numerical study of a modified time-stepping θ-scheme for incompressible flow simulations. J Sci Comput 28(2–3):533–547. doi:10.1007/s10915-006-9083-y
64. Turek S, Schäfer M (1996) Benchmark computations of laminar flow around cylinder. In: Flow simulation with high-performance computers II. Notes on numerical fluid mechanics, vol 52. Vieweg, Wiesbaden, pp 547–566
65. Unverdi SO, Tryggvason G (1992) A front-tracking method for viscous, incompressible, multi-fluid flows. J Comput Phys 100(1):25–37. doi:10.1016/0021-9991(92)90307-K
66. Veneziani A, Villa U (2011) ALADINS: an ALgebraic splitting time ADaptive solver for the incompressible Navier-Stokes equations. Part 1: basic settings and analysis. Technical report TR-2011-010, Emory University
67. Welch JE, Harlow FH, Shannon JP, Daly BJ (1966) The MAC method: a computing technique for solving viscous, incompressible, transient fluid-flow problems involving free surfaces. Los Alamos Scientific Laboratory Report LA-3425
68. Yu J-D, Sakai S, Sethian JA (2007) Two-phase viscoelastic jetting. J Comput Phys 220(2):568–585. doi:10.1016/j.jcp.2006.05.020
69. Zhao H (2005) A fast sweeping method for Eikonal equations. Math Comput 74(250):603–627